Bioinspiration & Biomimetics

RECEIVED
23 May 2024

REVISED
6 August 2024

ACCEPTED FOR PUBLICATION
23 August 2024

PUBLISHED
12 September 2024

PAPER

Comparison of feed-forward control strategies for simplified vertical hopping model with intrinsic muscle properties

Dóra Patkó[1,2,*] **and Ambrus Zelei**[3]

[1] Department of Applied Mechanics Faculty of Mechanical Engineering Budapest University of Technology and Economics, Műegyetem rkp. 3., H-1111 Budapest, Hungary
[2] MTA-BME Lendület 'Momentum' Global Dynamics Research Group Budapest University of Technology and Economics Műegyetem rkp. 3., H-1111 Budapest, Hungary
[3] Department of Whole Vehicle EngineeringAudi Hungaria Faculty of Automotive Engineering Széchenyi István University, Győr, Hungary
[*] Author to whom any correspondence should be addressed.

E-mail: dora.patko@mm.bme.hu

Keywords: vertical hopping, Hill muscle, piecewise-smooth periodic systems, dynamical integrity, reductionist approach

Abstract

To analyse walking, running or hopping motions, models with high degrees of freedom are usually used. However simple reductionist models are advantageous within certain limits. In a simple manner, the hopping motion is generally modelled by a spring-mass system, resulting in piecewise smooth dynamics with marginally stable periodic solutions. For a more realistic behaviour, the spring is replaced by a variety of muscle models due to which asymptotically stable periodic motions may occur. The intrinsic properties of the muscle model, i.e. preflexes, are usually taken into account in three complexities—constant, linear and Hill-type. In this paper, we propose a semi-closed form feed-forward control which represents the muscle activation and results in symmetrical hopping motion. The research question is whether hopping motions with symmetric force-time history have advantages over asymmetric ones in two aspects. The first aspect is its applicability for describing human motion. The second aspect is related to robotics where the efficiency is expressed in term of performance measures. The symmetric systems are compared with each other and with those from the literature using performance measures such as hopping height, energetic efficiency, stability of the periodic orbit, and dynamical robustness estimated by the local integrity measure (LIM). The paper also demonstrates that the DynIn MatLab Toolbox that has been developed for the estimation of the LIM of equilibrium points is applicable for periodic orbits.

1. Introduction

Pedal locomotion and its dynamics and control have been the focus of research in the recent decades. Mechanical models of hopping can vary from simple low degrees of freedom (DoF) [1–3] through multi-segmented models [4–6] to complex musculoskeletal models with high DoF [7–9]. In the former, the centre of gravity (CoG) is treated as a point mass, and the entire leg is modelled by a spring with damper [1, 4, 10, 11] or a muscle model [2, 3]. These models due to their low DoF and low computational effort are relatively easy to examine. Therefore it is practical to use low DoF models to get a preliminary picture of the effects of various parameters or control strategies [2, 3, 12, 13]. Pedal motion in general and especially hopping motion is mainly described by piece-wise smooth dynamics with periodic orbits as solution while the centre of mass oscillates vertically [12, 14, 15].

With musculoskeletal models, the roles and influence of different muscle groups have been investigated to obtain a deeper and more comprehensive understanding of the pedal locomotion [7]. A widely used muscle model is the Hill-type muscle [2, 3, 7, 9, 16]. The Hill-type model consists of an active contractile element (CE) and two passive elastic elements: one parallel and one serial to the CE [16]. Passive elastic elements model the elasticity of the muscle and the tendons [17]. The active element only capable

© 2024 IOP Publishing Ltd. All rights, including for text and data mining, AI training, and similar technologies, are reserved.

of exerting pulling type force, just as real muscles, and it has intrinsic force-length (f_l) and force-velocity (f_v) properties [16]. These relations modify the theoretical maximum of the force output depending on the current state of the muscle. These characteristics of the muscle are called preflexes since they act like zero-delay reflexes [18, 19]. The force-length and force-velocity relations are described by non-linear Hill-type functions [16], but sometimes are simplified by linear or constant functions. Hauefle *et al* [2] concluded that at least a linear force-velocity relation is needed to develop asymptotically stable periodic hopping.

The CE is considered an active element because it exerts force of a magnitude corresponding to the so-called *activation level* [20]. This means that the force output depends not only on the current length and contraction velocity of the muscle, but also on the activation level, which represents the nerve impulses coming from the nervous system. It describes the extent to which the muscle should be contracted. In the case of musculoskeletal models, the activation function is usually defined with the help of EMG data [9].

Since the Hill model includes the active element, a control algorithm is needed to determine the activation level of the muscle at each time instant. Feed-forward and/or feedback approaches may be used in the mathematical models of hopping motion. The physiological background of the feed-forward control is the *central pattern generator* (CPG), found in the spinal cord of vertebrates [19, 21–25]. The CPG forms a low level neuromuscular control and generates rhythmic patterns of motor activity, such as those involved in walking or hopping, without requiring constant input from the brain. Stable hopping can be achieved without cautiously focusing much on the motion. The supra-spinal layer of the neuromuscular activities [24] may be modelled by feedback control. Hauefle *et al* [3] found that in the case of a one DoF hopping model with a simplified Hill-type muscle, the combination of feed-forward and proprioceptive feedback control improved the hopping stability.

The stability of the hopping motion is mathematically determined by the eigenvalues of the so-called *monodromy matrix* of a periodic orbit [5, 26]. Besides local stability, the *basin of attraction* (BoA) serves also as a quite important characteristic of a solution, since perturbations can cause stability loss, and this information cannot be extracted from the monodromy matrix. To calculate the BoA of a solution is usually computationally intensive. Therefore several measures of dynamical integrity were defined to estimate the robustness of a solution [27–30]. Besides the BoA, these measures also provide valuable information on the robustness of solutions. Habib [31] introduced a rapid and efficient numerical algorithm developed in MatLab, the `DynIn` Toolbox, to estimate the *local integrity measure* (LIM) of an equilibrium point. The LIM is the maximal radius of a hypersphere in the phase space completely included within the BoA and centred at the equilibrium point [27]. Meaning that solutions started with initial conditions (ICs) within this hypersphere converge to the equilibrium point. Although the algorithm is developed for equilibrium points, it is also able to estimate the robustness of a periodic motion by computing the LIM of the fix point on a well-chosen Poincaré section.

In this study, we examine the effects of a predefined, closed-form activation function on a simple one DoF hopping model introduced by Hauefle *et al* [2]. In paper [2], the activation level of the single Hill muscle was obtained by using genetic algorithm. Preflexes, as considered in [2], are analysed with varying complexities, resulting in multiple systems. In [2], the complexity criteria of the preflexes was analysed for achieving stable hopping motion. On the contrary, in our work, a closed form activation function is chosen so that the CE behaves completely elastic during stable hopping, resulting in symmetric motion. In our paper, the effect of symmetry is analysed regarding the performance of the systems, which is measured through various performance measures. We hypothesize that the closed-form activation function is a feasible alternative for choosing the feed-forward control in modelling human hopping. This hypothesis is based on the finding of an experimental observation indicating that the ground reaction forces of human hopping motion can be modelled by a simple mass-spring system at preferred or higher frequencies [32]. However, the used muscle model is not sufficiently complex to study the underlying physiological phenomena related to the muscle behaviour or human hopping motion, since the elasticity of the muscle-tendon unit and the leg geometry are neglected, which have an important role in legged locomotion [33–35]. Additionally, this study addresses the implications for robotics.

However, we use measures defined in [2], we also introduce measures for a more complete comparison, such as performance measure of energy efficiency and measure related to the dynamical robustness of the stable solution. Moreover, the stability of the periodic orbits is analysed via the spectral radius of the monodromy matrix instead of using Poincaré return maps. We evaluate the advantages and disadvantages of systems with symmetric motion control focusing on stability, performance, convergence speed, and dynamical robustness with different levels of complexity in f_l and f_v. We demonstrate that the `DynIn` MatLab Toolbox developed by Habib [31], used for estimating the LIM of equilibrium points, is suitable for assessing the robustness of a fix point of periodic orbits. Our goal is to compare the performance of the models

using the proposed closed-form activation with each other and with the systems in [2], whose activation functions were calculated by a meta-heuristic optimization algorithm.

2. Methods

2.1. Mechanical model of vertical hopping

The mechanical model shown in figure 1 is based on the work of Hauefle *et al* [2]. The CoG is modelled by a point-mass which includes the mass of the whole body, and it is supported by a simplified Hill-type muscle only consisting of the CE. During motion, the flight, divided into upwards and downwards phases, and stance phases alternate. The t_{D2S} is the time instant when the downwards moving mass is at distance l_0 from the ground, therefore when the straightened leg touches the ground. This event is called touch down. The t_{S2U} is the time instant, when the mass is once again at distance l_0 from the ground, therefore when leg becomes fully straightened again. This event is called take-off. Since the muscle have to work against the gravity, and it is only capable to exert pulling force, the muscle model has to be inverted. As it can be seen, the mass move upwards if the muscle is contracted.

The force output of the muscle is described by the equation

$$F_{\mathrm{out}}(t,y,\dot{y}) = F_{\max}\, a(t)\, f_l(y)\, f_v(\dot{y}), \tag{1}$$

where $F_{\max}$ is the theoretical maximum force the muscle can exert, and $a(t)$ is the activation level defined by the control. The preflex related multipliers $f_l(y)$ and $f_v(\dot{y})$ are functions of contraction y and contraction-speed $\dot{y}$. These preflex-related intrinsic characteristics only depend on the contraction and the contraction speed, since the whole leg is modelled by a single Hill muscle.

The intrinsic f_l and f_v relations of the Hill muscle model are described by non-linear Hill functions. However, they can be simplified by using linear or constant functions. Both for f_l and f_v it is possible to introduce constant, linear or non-linear functions resulting nine possible combinations of equation (1). Hauefle *et al* concluded in their work that if the system has at least first order (i.e. linear) f_v relation, periodic orbits with asymptotic stability can be found [2]. Since we are interested in the robustness of periodic orbits, systems with constant f_v are not considered among the nine combinations from [2]. The reason is that constant f_v does not lead to asymptotically stable periodic orbit only marginally stable. In this work, the functions describing the intrinsic properties in the case of different complexities are

$$f_l(y) = \begin{cases} 1 & \text{constant,} \\ k(l_0 - y) & \text{linear,} \\ \exp\left(c\left|\frac{y-l_{\mathrm{opt}}}{w l_{\mathrm{opt}}}\right|^3\right) & \text{Hill,} \end{cases} \tag{2}$$

$$f_v(\dot{y}) = \begin{cases} 1-\mu\dot{y} & \text{linear,} \\ \begin{cases} \frac{v_{\max}+\dot{y}}{v_{\max}-K\dot{y}} & v>0 \\ N+(N-1)\frac{v_{\max}-\dot{y}}{-7.56K\dot{y}-v_{\max}} & v\leqslant 0 \end{cases} & \text{Hill.} \end{cases} \tag{3}$$

The graph of the functions is shown in figure 2. The Hill type f_l function can take values between 0 and 1. It takes the value 1 at the optimal length l_{opt} of the muscle. In the linear case, the k constant is chosen in such way that the function have value 1 at muscle length of l_{opt} also. The f_v functions can take values higher than 1 in the case of eccentric contraction and they take the value 1 at zero contraction velocity $\dot{y} = 0$. Since the muscle is inverted, the model has eccentric contraction when the mass moves downwards, therefore the CE can produce higher forces at negative $\dot{y}$ values.

The parameters of the system are collected in table 1. The values were chosen according to [2]. The parameter c describing the curvature of the bell-shaped Hill function is determined such that the value of f_l in equation (2) is 0.8 at l_0 muscle length [2].

2.2. Activation level for the Hill type muscle model

Control strategies are examined through the activation level. The model includes only a low level feed-forward control representing the CPG [20]. Due to the repetitive nature of the uniform elevation hopping motion, we assume that higher level control is not necessary. Since the gravitational field is potential, the mechanical energy of the system is constant in the flight phase. Therefore, the existence of periodic motion depends on the behaviour of the system in the stance phase; the muscle is responsible to reverse the motion of the mass by absorbing its kinetic energy and after that regenerating the absorbed energy while pushing the mass upwards.

Our goal was to determine a predefined activation function $a(t)$ for which there exists a stable periodic motion and the muscle behaves completely elastic while moving on this periodic orbit. In other words, the force-time history of the solution is symmetric in time. The elasticity coefficient, according to [36] is

$$C_{\mathrm{EL}} = \left(1 - \frac{D}{D_{\max}}\right)^2, \tag{4}$$

where D is the net hysteresis area enclosed by the contraction-force trace and it is normalized by $D_{\max}$, the product of the maximal force and maximum contraction. The higher the C_{EL} value, the more elastic

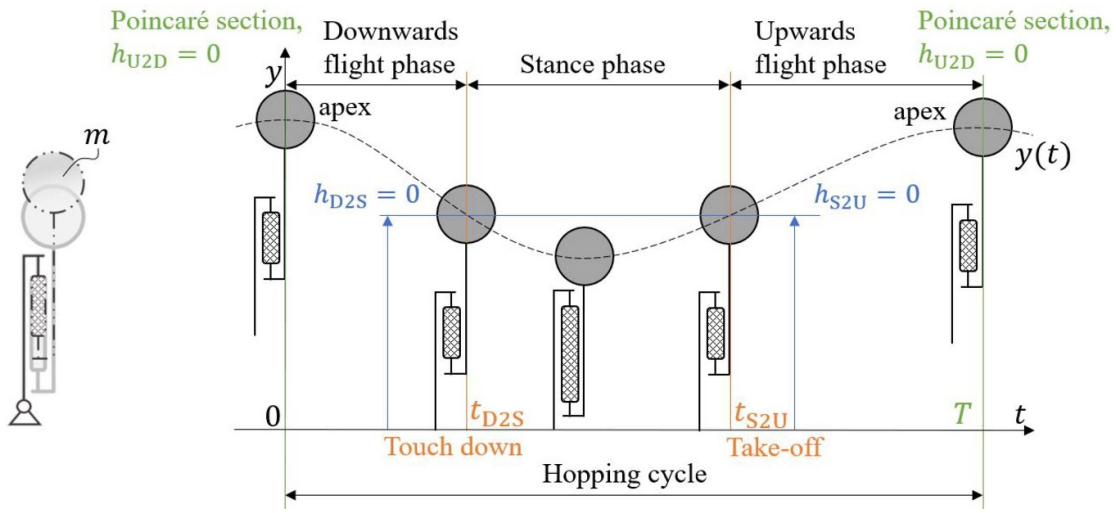

Figure 1. Hopping cycle of the one DoF hopping model.

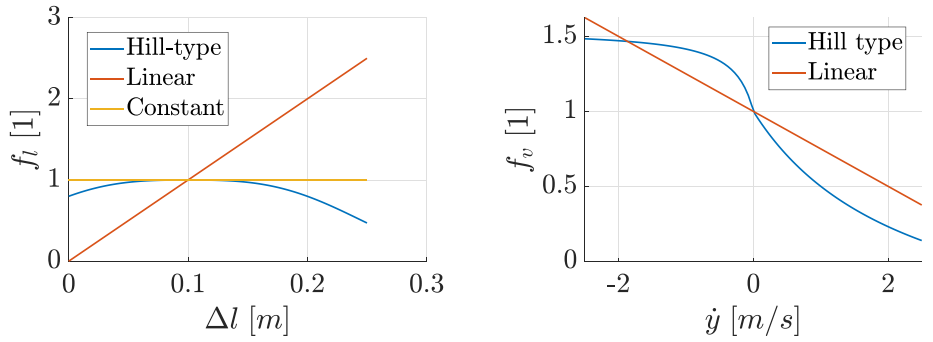

Figure 2. Intrinsic muscle properties of different complexities.

Table 1. Parameters of the mechanical model. Adapted from [2]. © IOP Publishing Ltd. All rights reserved.

Notation	Parameter	Value	Dimension
l_0	Leg length	1	m
m	Mass	80	kg
g	Gravitational acceleration	10	$\mathrm{m\,s^{-2}}$
F_{max}	Maximal muscle force	2.5	kN
l_{opt}	Optimal muscle length	0.9	m
w	Width of the Hill bell-shaped curve	0.45	1
v_{max}	Maximal contraction velocity	−3.5	$\mathrm{m\,s^{-1}}$
K	Curvature parameter of the Hill f_v function	1.5	1
N	Eccentric force enhancement parameter	1.5	1
k	Spring constant of linear f_l relation	10	$1/\mathrm{m}$
μ	Slope of the linear f_v relation	0.25	$\mathrm{s\,m^{-1}}$

the behaviour of the muscle. In the case of completely elastic behaviour, there is no hysteresis in the contraction-force relation and therefore $C_{EL} = 1$. The value of C_{EL} is used to indicate that the resulting motion is truly completely elastic.

The objective in this paper is to define the activation function $a(t)$ in such way that it i) results in a periodic orbit, ii) cancels out the effects that would cause hysteresis, i.e. the goal is $C_{EL} = 1$. The $f_v(\dot{y})$ relation (3) is not symmetric to the zero contraction speed $\dot{y} = 0$, meanwhile the $f_l(y)$ values defined by equation (2) are the same while contracting and extracting at the corresponding muscle lengths. Therefore, in the specific case where f_v and $a(t)$ are constant, the force output F_{out} is the same for concentric and eccentric contractions for any amongst the introduced f_l relations in equation (2). Meaning, that there is no hysteresis. However, if the f_v is defined

by equation (3), the force output is lower for concentric contraction than for eccentric contraction as the effect of the f_v. Therefore the intrinsic cause of the hysteresis D in equation (4) is the f_v function. Thus, we hypothesize that the following function would be a good choice for the activation level $a(t)$ to eliminate the effect of function f_v

$$a_{\mathrm{S}}(t) = \frac{1}{f_v\left(\dot{y}_{\mathrm{per}}(t)\right)\kappa}. \tag{5}$$

Here, $\dot{y}_{\mathrm{per}}(t)$ is the velocity of the mass assuming periodic orbit. The scalar variable κ is an arbitrary constant so the activation function $a_{\mathrm{S}}(t) \in [0, 1]$ is fulfilled for any time instant t. Choosing $a_{\mathrm{S}}(t)$ based on equation (5) results *symmetric* $F_{\mathrm{out}}(t)$ time histories for periodic motions, as it cancels out the effect of f_v by substituting into equation (1):

$$F_{\mathrm{out,S}}(t, y, \dot{y}) = F_{\max} f_l(y) \frac{f_v(\dot{y})}{f_v\left(\dot{y}_{\mathrm{per}}(t)\right)\kappa}. \tag{6}$$

Although, in equation (5), the prior knowledge of the periodic motion is expected, such $a_{\mathrm{S}}(t)$ functions are easy to find numerically. One can take advantage of the fact that these one dimensional hopping systems with $f_v(\dot{y}) \equiv \text{const.}$ are always marginally stable with any ICs, since they are conservative [2]. Therefore, by choosing $f_v(\dot{y}) = 1$ and $a(t) = 1/\kappa$, with an initial guess for κ, in the force output $F_{\mathrm{out}}(t, y, \dot{y})$ in equation (1), a periodic motion $y_{\mathrm{PerC}}(t)$ is obtained for an arbitrary IC:

$$\begin{aligned} F_{\mathrm{out,PerC}}(y) &= F_{\max} f_l(y) \frac{1}{\kappa}, \\ y(0) &= y_0, \\ \dot{y}(0) &= \dot{y}_0. \end{aligned} \tag{7}$$

After that, $a_{\mathrm{S}}(t)$ is generated by substituting the obtained function $\dot{y}_{\mathrm{PerC}}(t)$ in equation (5) as the $\dot{y}_{\mathrm{per}}(t)$ term. The same $y_{\mathrm{PerC}}(t)$ periodic motion is realized with the original $f_v(\dot{y})$ from equation (3) as with $f_v(\dot{y}) = 1$ and $a(t) = 1/\kappa$. The reason behind this phenomenon is that, by starting the system from the IC used in equation (7), the force output in equation (6) is the same as in equation (7), since at any given time instance τ the value of $f_v(\dot{y}(\tau))$ will be equal to the defined $f_v(\dot{y}_{\mathrm{PerC}}(\tau))$.

Since $a_{\mathrm{S}}(t) \in [0, 1]$ is required, one needs to check whether the maximum of $a_{\mathrm{S}}(t)$ is not higher than 1. If $\max(a_{\mathrm{S}}(t)) < 1$, the activation function is ready to use. However, if $1 < \max(a_{\mathrm{S}}(t))$, the above $y_{\mathrm{PerC}}(t)$ motion cannot be realized. In this case, the κ value in $a(t) = 1/\kappa$ must be increased. This makes the magnitude of the muscle forces lower while calculating the periodic orbit of the conservative system. This process is repeated with higher κ values until $\max(a_{\mathrm{S}}(t)) \leqslant 1$ is met.

2.3. Piece-wise smooth dynamics of the mechanical model

The dynamics of the system is piece-wise smooth, consisting of consecutive flight and stance phases, as figure 1 shows. The equation of motion (EoM) in the stance phase is

$$\ddot{y} = \frac{F_{\mathrm{out}}(t)}{m} - g. \tag{8}$$

In the flight phase, $F_{\mathrm{out}}(t)$ is zero. The gravitation acts only on the point-mass m. The problem is two-dimensional described by y and $\dot{y}$, and due to the presence of the explicitly time-dependent $a(t)$ function, the system is non-autonomous.

The feed-forward control is determined for each period of hopping through the activation level $a(t)$. Therefore the time parameter in the predefined function $a(t)$ resets at the beginning of each period. Thus, the explicit feed-forward control has a state-dependent reset condition. This makes necessary to introduce a new variable t_a, which represents the internal time status of the controller. According to [2], let us choose the new period event at the apex of the flight phase and define a Poincaré section there. The corresponding event function [26, 37, 38], which defines the Poincaré section, where the mass starts to move downwards, is $h_{\mathrm{U2D}}(\mathbf{z}) = 0$:

$$h_{\mathrm{U2D}}(\mathbf{z}) = \dot{y}. \tag{9}$$

Handling the time as a state variable is not only necessary because of the state-dependent nature of the controller, but also advantageous, since the originally non-autonomous system is transformed into an autonomous one, if the time in the activation level is included in the state variables [26]. As a consequence, a three-dimensional problem emerges with

$$\mathbf{z} = \begin{bmatrix} y & \dot{y} & t_a \end{bmatrix}^{\mathrm{T}}, \tag{10}$$

and the activation $a(t_a)$ is the function of t_a:

$$t_a = t - t_{\mathrm{U2D}}, \tag{11}$$

where t_{U2D} is the preceding time instant when the Poincaré section (i.e. the beginning of a new period) is reached. Indices U and D refer to the phase transition from upwards to downwards motion. Practically, the t_a variable is mapped to zero as the mass reaches the apex, introducing a discontinuity in the flight phase. Since $a(t_a)$ resets at the Poincaré section [2, 36], the mapping function [26, 37, 38] at the event, defined in equation (9), is

$$\mathbf{g}_{\mathrm{U2D}} = \begin{bmatrix} y & \dot{y} & 0 \end{bmatrix}^{\mathrm{T}}. \tag{12}$$

Due to the mapping of the t_a, all state variables remain periodic.

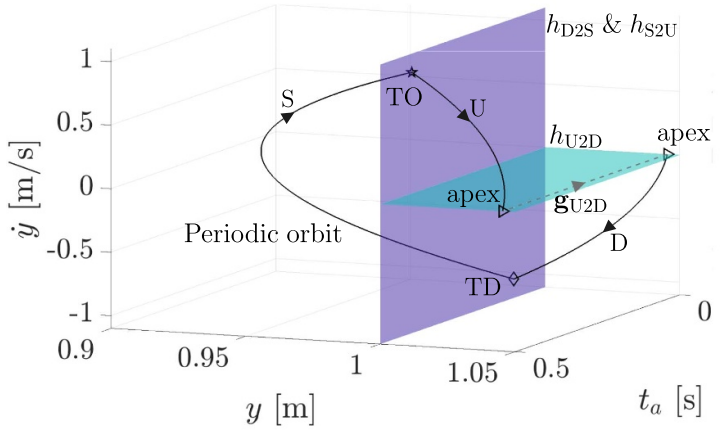

Figure 3. Illustration of a periodic trajectory in the phase space, considering t_a as state variable. Touch down and take-off are denoted by TD and TO respectively. The $\mathbf{g}_{U2D}$ function maps the time t_a to zero after the trajectory reaches the Poincaré section.

As figure 3 shows, the event functions for the downwards flight to stance (D2S) phase transition $h_{D2S}(\mathbf{z}) = 0$ and the stance to upwards flight (S2U) phase transition $h_{S2U}(\mathbf{z}) = 0$ are

$$h_{D2S}(\mathbf{z}) = l_0 - y, \tag{13}$$

$$h_{S2U}(\mathbf{z}) = l_0 - y, \tag{14}$$

where l_0 is the rest length of the leg (see table 1). Since in the stance phase the mass connects to the ground through a spring, there is no impact at the touchdown and the solutions have at least C^1 continuity. Therefore the mapping functions $\mathbf{g}_{D2S}(\mathbf{z}) = \mathbf{z}$ and $\mathbf{g}_{S2U}(\mathbf{z}) = \mathbf{z}$ are identities and transform everything into its own image after phase transitions. In figure 3, an illustrative example of the periodic trajectory can be seen in the three-dimensional state space.

During simulations, the EoM in the flight phase is solved analytically:

$$y_{Flight}(t_0 + \tau) = y_0 + \dot{y}_0 \tau - \frac{1}{2} g \tau^2, \tag{15}$$

where the global time is $t = t_0 + \tau$. The time instants at the apex t_{U2D} and at the downwards flight to stance transition t_{D2S} are, respectively:

$$t_{U2D} = t_0 + \frac{\dot{y}_0}{g}, \tag{16}$$

$$t_{D2S} = t_0 - \frac{\sqrt{2g(y_0 - l_0) + \dot{y}_0^2}}{g}. \tag{17}$$

Generally, there is no analytic solution for the EoM in the stance phase. Therefore, in this case, the EoM is solved by using MATLAB `ode45`, and the phase transition, which occurs at the t_{S2U} time instant, was identified by the MATLAB ode45 numerical event handler using equation (14).

2.4. Stability analysis via monodromy matrix

For an initial value problem of an autonomous smooth system, the stability of a solution is described by the eigenvalues of the Jacobian of the flow [26]. The fundamental matrix is calculated by solving the first variational equation with the initial value problem

$$\begin{cases} \dot{\mathbf{z}}(t) = \mathbf{f}(\mathbf{z}(t)), \\ \mathbf{z}(t_0) = \mathbf{z}_0, \\ \dot{\mathbf{\Phi}}(t) = \left.\frac{\partial \mathbf{f}(\mathbf{z})}{\partial \mathbf{z}}\right|_{\mathbf{q}_{per}} \mathbf{\Phi}(t), \\ \mathbf{\Phi}(t_0) = \mathbf{I}, \end{cases} \tag{18}$$

where t_0 is chosen freely without being bound by generality, as the system is autonomous, $\mathbf{I}$ is the identity matrix, $\mathbf{\Phi}$ is the fundamental matrix and $\mathbf{f}(\mathbf{z}(t))$ is the smooth vector field. In the case of a periodic solution, the fundamental matrix calculated between t_0 and $t_0 + T$, where T is the period time, is called monodromy matrix $\mathbf{M}$. The eigenvalues of $\mathbf{M}$ are the Floquet multipliers and they determine the stability of the periodic orbit.

However, the system is a non-smooth hybrid system of which the solution contains continuous flows interconnected by discrete mappings. Therefore, separate fundamental matrix is calculated for each continuous phase. The monodromy matrix is determined by multiplying these fundamental matrices while correcting them with the saltation matrices ($\mathbf{S}_{U2D}$, $\mathbf{S}_{D2S}$ and $\mathbf{S}_{S2U}$) at each phase change [26, 37–39]. The formalization of the saltation matrix is rigorous and depends on the governing EoM of the phases it links together, the mapping at the phase change and the event function indicating the phase change. Since the system has three consecutive continuous phases, three saltation matrices are needed. However, we only introduce one of these three matrices since the construction of the other two matrices is identical. The saltation matrix at the upwards to downwards flight phase transition has the following form [26, 37, 38]:

$$\mathbf{S}_{\mathrm{U2D}} = \mathbf{g}_{\mathrm{U2D},\mathbf{z}}\left(t^{-}_{\mathrm{U2D}}\right) + \frac{\left(\mathbf{f}\left(\mathbf{z}\left(t^{+}_{\mathrm{U2D}}\right)\right) - \mathbf{g}_{\mathrm{U2D},\mathbf{z}}\left(t^{-}_{\mathrm{U2D}}\right)\mathbf{f}\left(\mathbf{z}\left(t^{-}_{\mathrm{U2D}}\right)\right)\right)\mathbf{h}_{\mathrm{U2D},\mathbf{z}}\left(t^{-}_{\mathrm{U2D}}\right)}{\mathbf{h}_{\mathrm{U2D},\mathbf{z}}\left(t^{-}_{\mathrm{U2D}}\right)\mathbf{f}\left(\mathbf{z}\left(t^{-}_{\mathrm{U2D}}\right)\right)}, \tag{19}$$

where the + and − signals in the upper index indicate whether the expression is calculated infinitesimally small time duration before or after the time instant of the phase change, and the **z** in the lower index means that the term is differentiated by the state variables. The saltation matrices $\mathbf{S}_{\mathrm{D2S}}$ and $\mathbf{S}_{\mathrm{S2U}}$ are also necessary and are calculated analogously to equation (19).

In the case of a non-smooth system, the monodromy matrix is constructed by calculating the fundamental matrix (18) at the respective phase of the system, and at phase change, the fundamental matrix is multiplied by the saltation matrix governing the phase transition. After that, integration of the fundamental matrix in the new phase is needed, which is later used to multiply the previously obtained matrix. Assuming that the solution is started from the Poincaré section, the monodromy matrix is calculated as [5, 26, 37, 38]:

$$\mathbf{M} = \mathbf{S}_{\mathrm{U2D}}\,\mathbf{\Phi}_{\mathrm{U}}\left(t^{-}_{\mathrm{U2D}}\right)\mathbf{S}_{\mathrm{S2U}}\,\mathbf{\Phi}_{\mathrm{S}}\left(t^{-}_{\mathrm{S2U}}\right)\mathbf{S}_{\mathrm{D2S}}\,\mathbf{\Phi}_{\mathrm{D}}\left(t^{-}_{\mathrm{D2S}}\right). \tag{20}$$

At the end, the saltation matrix for the upwards to downwards phase transition is required since the system restarts again in the downwards phase. The stability is determined by the spectral radius of **M** while ignoring the trivial multiplier of value 1 with the corresponding eigenvector of $\mathbf{f}(\mathbf{z}(t_0)) \equiv \mathbf{f}(\mathbf{z}(t^{+}_{\mathrm{U2D}}))$. Hence the time is included in the state variables to make the system autonomous, an extra trivial multiplier occurs [26] with value 0, since the time t_a is mapped to zero at the Poincaré section. If the spectral radius of **M**, excluding the trivial eigenvalues, is lower than one, the periodic orbit is asymptotically stable [26]. In this three-dimensional problem, there is a single non-trivial multiplier.

Since the activation level resets at the Poincaré section, the system can be examined as a one-dimensional problem on the Poincaré section via the Poincaré return map as it was done by Hauefle *et al* [2]. This approach is used to examine the behaviour of the system graphically. The fix points of the return map are the periodic solutions of the system. The stability of a periodic solution is described by the slope of the curve at the fix point. The slope of the curve and the non-trivial eigenvalue of **M** are equal. An advantage of the Poincaré return map is that the BoA of a fix point on the Poincaré section is also readable from the figure. However, this information about the BoA of the solution would be limited, since the problem is three-dimensional.

2.5. Dynamical robustness via LIM

Non-linear dynamical systems have limited robustness against external perturbations [40]. The BoA of a stable solution tells us how robust it is against disturbances. However, determining the exact BoA is a computationally expensive task, especially for systems with high dimensions. In the literature, several dynamical integrity measures were introduced to quantify the dynamical robustness [27, 28]. Habib [31] developed the `DynIn` Toolbox in MatLab, which provides an upper estimate of the LIM of a stable equilibrium point [27].

Although, the `DynIn` Toolbox was originally developed for equilibrium points, we aim to use this iterative algorithm for periodic orbits exploiting that on the Poincaré section the fix point is treated as an equilibrium point of a discrete mapping [31]. The `DynIn` Toolbox uses numerical integration and discretizes the trajectory to examine the behaviour of a solution. In each iteration step a numerical solution is examined through sampling points of its discretization. The LIM is the minimal distance (i.e. hypersphere radius) between the fix point and the closest diverging point. The resulting LIM estimates the radius of the largest hypersphere centred at the fix point, that is completely inside of the BoA of the stable periodic solution [27, 31].

The dimension of the hypersphere was considered according to three approaches, as shown in figure 4. In 1D, 2D and 3D, the notations are LIM_1, LIM_2 and LIM_3 respectively. In the case of the 1D approach, when the hypersphere is a line, the ICs were chosen on the Poincaré section. Therefore, while choosing the ICs, variables $\dot{y}$ and t_a were fixed as zeros and y was varied. Since the Poincaré section is in the flight phase, the initial y is chosen in the flight phase, i.e. the flight to stance transition limits from below the eligible y values as ICs. The result of this approach corresponds to the BoA read from the Poincaré return map mentioned in section 2.4.

Since the systems have feed-forward control with state dependent reset condition, the effect related to errors of state perception is worth investigating. For this reason, the 2D and 3D approaches are introduced where the hypersphere are respectively a circle and a sphere. The perceptional error of the control means that the h_{U2D} transition is not detected correctly for the first hopping cycle. After the first h_{U2D} transition,

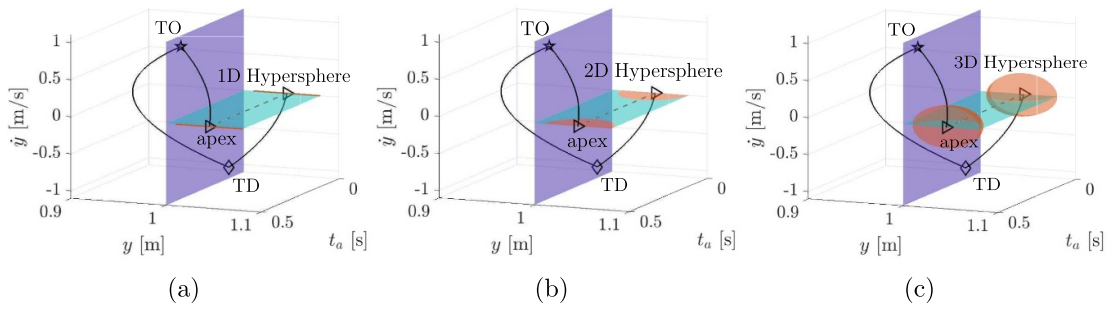

Figure 4. Illustration of the hypersphere of different dimensions: (a) LIM_1 for 1D, (b) LIM_2 for 2D, (c) LIM_3 for 3D approaches.

the controller is able to detect the apex point of the flight phase. The perceptional error is taken into account by perturbing the t_a variable. Therefore in the case of the 2D approach only $\dot{y}$ has fix zero value while selecting the IC on the $y - t_a$ sub-phase plane. In the 3D case all three state variables are perturbed. In the 2D and 3D cases, the IC is no longer on the Poincaré section, i.e. the eligible y values are extended to be lower than l_0. The sampling points of the trajectory remain on the Poincaré section during the iterative algorithm of the `DynIn` Toolbox. The 2D and 3D approaches require more simulations to get accurate LIM estimations compared to the 1D approach because of the higher dimensional space.

2.6. Performance measures

Depending on the feed-forward control function, multiple solutions exist. Haeufle *et al* [2] used the following fitness function in a genetic algorithm to find the activation function $a(t)$, resulting in $a_{\mathrm{H}}(t)$:

$$P_{\mathrm{H}} = \begin{cases} \hat{y}_{\max} & T \leqslant 0.5\,\mathrm{s} \\ 2\hat{y}_{\max}\left(1 - \hat{T}\right) & T > 0.5\,\mathrm{s} \end{cases} \tag{21}$$

where the index H denotes to activation function used by Haeufle *et al*, $\hat{T}$ is the actual time period of hopping normalized by 1 s, and $\hat{y}_{\max}$ is the height of the mass from the ground at the apex of the flight phase normalized by 1 m. The function P_{H} ensures the highest hopping for 2 Hz frequency, which corresponds to the preferred human hopping frequency [2, 32, 41]. Since we aim to compare the control approaches, we also maximised the fitness function (21) while searching for the closed form $a_{\mathrm{S}}(t)$ using the theory introduced in section 2.2.

Additionally, we introduce the energy consumption of the muscle as a quantitative measure. The energetic cost of the muscle in each hopping period is calculated by integrating the absolute value of the power of the CE [16, 42]:

$$W_{\mathrm{CE}} = \int_{t_0}^{t_0+T} |F_{\mathrm{out}}\,\dot{y}|\ \mathrm{d}t, \tag{22}$$

where F_{out} is the force output of the CE as shown in equation (1). The performance measure P_{W} is defined as the ratio of the potential function of the mass at the apex height $y_{\max}$ measured from l_0 elevations and the energetic cost of the muscle

$$P_{\mathrm{W}} = \frac{mg\,(y_{\max} - l_0)}{W_{\mathrm{CE}}}. \tag{23}$$

The higher the value of P_{W} is, the greater part of the muscle work is used to earn a unit of potential energy surplus during hopping.

3. Results

The goal of this paper is to compare the properties of the newly proposed activation control, which results in a symmetric force-time history (see section 2.2), with the corresponding systems by Haeufle *et al* [2]. The newly proposed systems will be referred as *symmetric* and the systems from [2] will be called as *asymmetric* henceforth. Six combination of preflex-related multipliers are considered, as section 2.1 describes: constant, linear or Hill type force-length relation $f_l(y)$ in equation (2) combined with linear or Hill type force-velocity relation $f_v(\dot{y})$ in equation (3). The simulation results from [2] were regenerated and included in section 3 for those six systems which allows asymptotic stability. Apart from the performance measure P_{H}, additional measures are the LIM values and the energetic ratio P_{W} in this paper.

3.1. Periodic motions according to activation levels

A hopping cycle is illustrated in figure 5 for each system, displaying the oscillation of the mass, the force exerted by the CE, and the activation function. For systems with $a_{\mathrm{S}}(t)$ activation, the force-time and displacement-time histories are symmetric and the shape of the force function depends solely on the $f_l(y)$ type. Systems with Hill-type $f_v(\dot{y})$ relations have a breakpoint (denoted by BP in the graphs) in their $a_{\mathrm{S}}(t)$ functions when the mass is at its minimum y position in the stance phase. This phenomenon is the result of the breakpoint in the $f_v(\dot{y})$ relation shown in figure 2 right. In all cases, the activation is lower

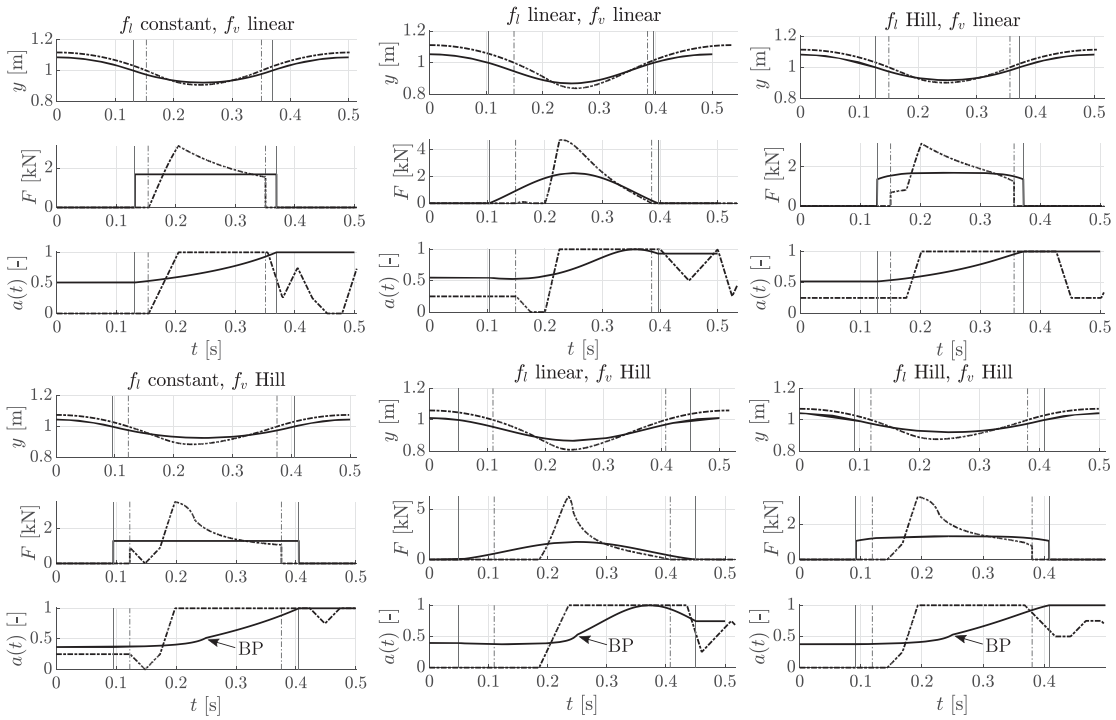

Figure 5. A hopping cycle for different systems; solid lines are denoted to the symmetric systems, dashed lines are denoted to the asymmetric systems, which are adapted from [2]. © IOP Publishing Ltd. All rights reserved. The vertical lines denote the beginning and the end of the stance phase.

at the beginning of the stance phase. Since the CE is inverted, the muscle has eccentric contraction when the mass is moving downwards. Therefore it is able to exert higher forces compared to the concentric contraction period, where higher activation is needed for the same force value. This phenomenon is originated in the non-symmetric nature of the force-velocity relation $f_v(\dot{y})$.

Symmetric systems (i.e. $a_S(t)$ control) have lower hopping heights, but approximately the same hopping frequencies as the corresponding asymmetric systems (i.e. $a_H(t)$ control, [2]), and therefore the air-ground ratio is less for the symmetric systems. Meaning, symmetric systems spend less time in air and more time on the ground actively using their muscle.

The values of hopping height (y_{max}), frequency (f) and Floquet multiplier (μ) are shown in table 2 in addition to the local integrity and performance measures introduced in section 2.5 and section 2.6 respectively. The value of the single non-trivial Floquet multiplier is equal to the slope of the curve at the respective fix point in the Poincaré return map, shown in figure 6. All hopping motion have asymptotic stability since $|\mu| < 1$ for all cases. The Floquet multiplier μ is positive for symmetric systems and negative for the asymmetric ones. Floquet multipliers $\mu < 0$ result in oscillatory convergence, which is in correspondence with the Poincaré return maps in figure 6.

3.2. Performance measures

The performance of the system is analysed through two measures P_H and P_W respectively related to the height of the hopping and to the energy consumption properties, these are shown in table 2. Asymmetric systems (i.e. [2]) have higher P_H values except for the system with linear-linear $f_l - f_v$ relation. This is not caused by higher y_{max}, but by the fact that the time period T is closer to 0.5 s (see equation (21)) for the symmetric system.

The mechanical energetic cost of the muscle (W_{CE}) is lower for symmetric systems, since the muscle behaves completely elastic during the periodic motion, as the C_{EL} shows in table 2. Still, the P_W values are greater for asymmetric systems, as the potential energy surplus is significantly greater. In general the difference in the P_W is marginal except for the systems with linear f_l properties.

The mechanical energetic cost is generally related to hysteresis in the contraction-force space. Therefore the muscle contraction-force curves are visualized in figure 7. The asymmetric systems have to regenerate the energy amount lost due to the hysteresis caused by the f_v property of the muscle, which is eliminated for the symmetric systems with activation function $a_S(t)$. Therefore symmetric systems with $a_S(t)$ control do not have hysteresis in their contraction-force relation while moving on the periodic orbit. The muscle absorbs energy (see in panel (a) of figure 8)

Table 2. Results of symmetric and asymmetric systems: hopping height and frequency, Floquet multiplier, elasticity coefficient, mechanical work of the muscle, performance measures and the LIM values of different dimensions are shown for each system.

	f_l	cons.		lin.		Hill	
f_v	Parameter	Symm.	Asymm.	Symm.	Asymm.	Symm.	Asymm.
lin.	y_{max} [m]	1.086	1.117	1.054	1.111	1.082	1.113
	f [Hz]	2	1.99	2	1.87	2	1.97
	μ [1]	0.85	−0.93	0.55	−0.85	0.79	-0.41
	C_{EL} [1]	1	0.599	1	0.664	1	0.626
	W_{CE} [J]	262	336	295	435	262	337
	P_H [1]	1.086	1.109	1.054	1.035	1.082	1.098
	P_W [1]	0.262	0.28	0.145	0.204	0.249	0.268
	LIM_1 [1]	0.0583	0.1174	0.0535	0.1112	0.071	0.1129
	LIM_2 [1]	0.0585	0.2419	0.0815	0.1364	0.0715	0.0865
	LIM_3 [1]	0.0588	0.2415	0.082	0.1376	0.0724	0.0865
Hill	y_{max} [m]	1.045	1.075	1.012	1.06	1.042	1.071
	f [Hz]	2	2.01	2	1.93	2	2
	μ [1]	0.89	−0.02	0.4	−0.53	0.75	−0.19
	C_{EL} [1]	1	0.579	1	0.767	1	0.541
	W_{CE} [J]	190	305	231	400	193	309
	P_H [1]	1.045	1.075	1.012	1.024	1.042	1.071
	P_W [1]	0.19	0.198	0.042	0.12	0.176	0.183
	LIM_1 [1]	0.0285	0.0754	0.0122	0.0601	0.0423	0.0706
	LIM_2 [1]	0.0269	0.544	0.031	0.0655	0.1616	0.0381
	LIM_3 [1]	0.0309	0.5447	0.0312	0.0662	0.1618	0.0381

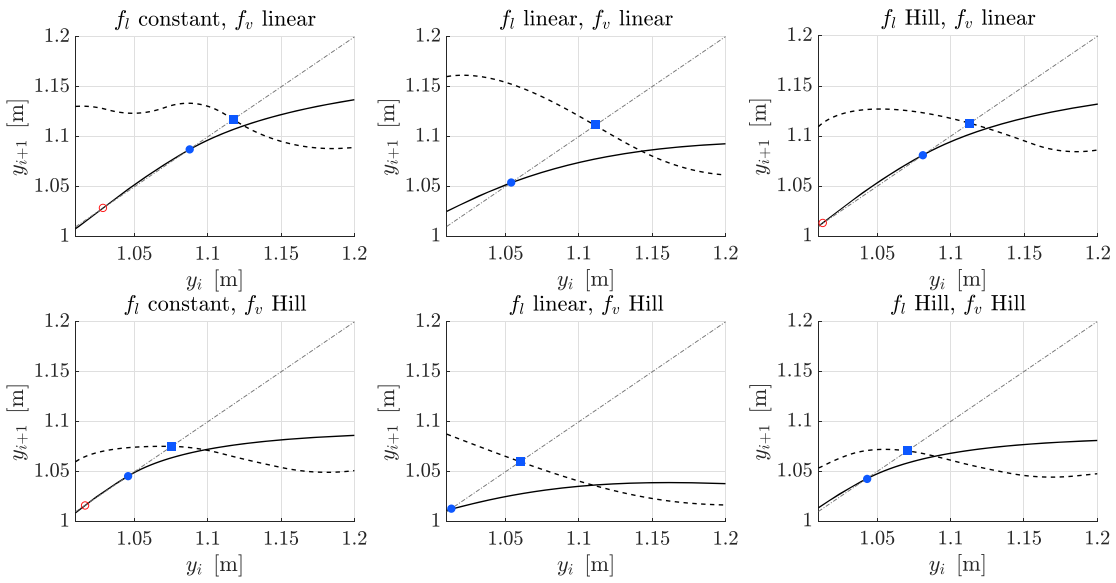

Figure 6. One-dimensional Poincaré return maps of systems. Solid lines represent symmetric systems with $a_S(t)$ control, while dashed lines represent asymmetric systems with $a_H(t)$ control adapted from [2]. © IOP Publishing Ltd. All rights reserved. Stable fixed points are indicated by blue filled markers, and unstable fixed points are indicated by red hollow markers.

or generates additional energy (see in panel (b) of figure 8) when the initial position is higher or lower than the apex of the periodic orbit respectively. The hysteresis decreases with each hopping cycle as it is shown in figure 8.

3.3. LIMs

Table 3 shows the optional inputs of the `DynIn` Toolbox used for calculating the LIM, which characterizes the dynamical robustness of a system. Higher hypersphere dimensions require more iteration steps. The distances measured along the y, t_a, and $\dot{y}$ directions are weighted by $1\,m^{-2}$, $1\,s^{-2}$, and $1\,s^2\,m^{-2}$, respectively, to determine the dimensionless radius of the hypersphere. Table 2 presents the estimate of the LIM values for different hypersphere dimensions.

Since the 1D approach is only considered in the flight phase, significant differences are noticeable between the values of LIM_1 comparing to LIM_2 and LIM_3. The values of LIM_2 and LIM_3 are close to

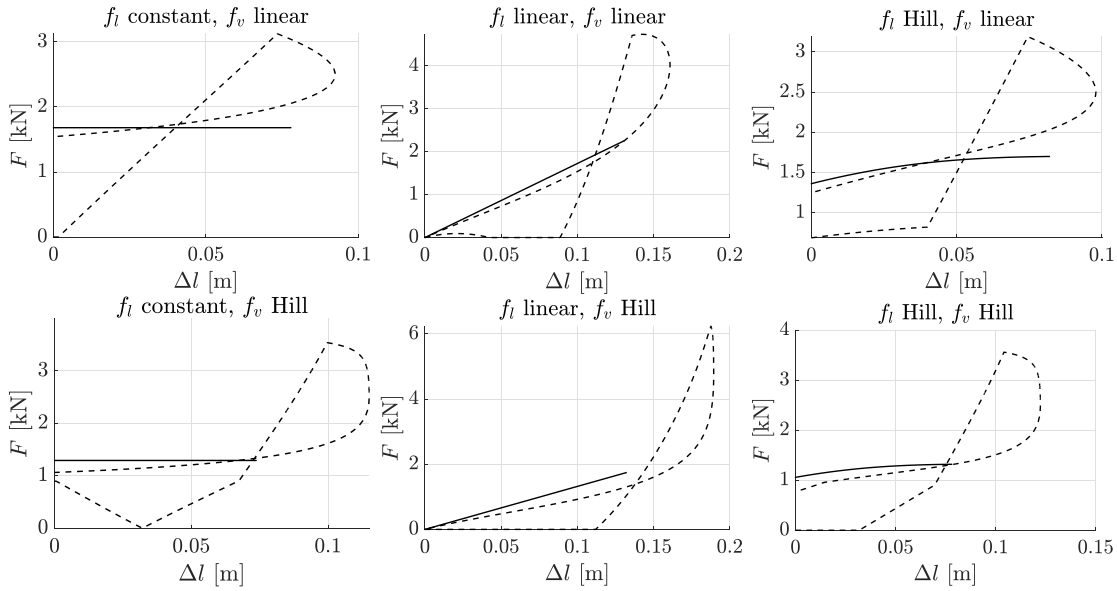

Figure 7. Exerted force against muscle contraction. Solid lines denote to symmetric systems, dashed lines denote to asymmetric systems.

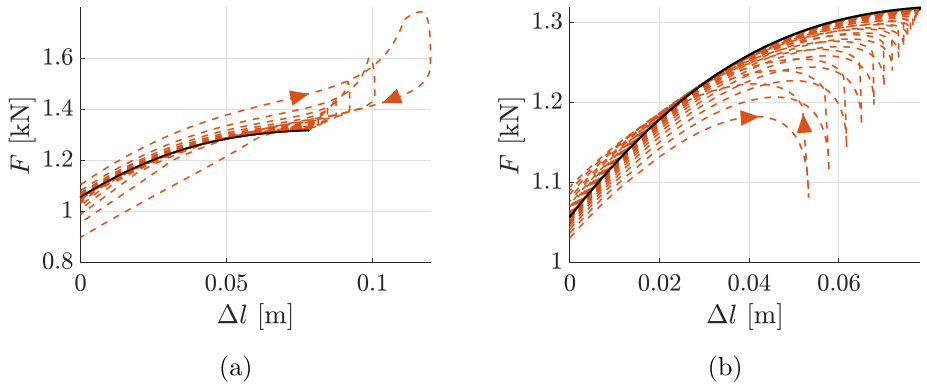

Figure 8. Muscle contraction-force curves for the symmetric system with Hill-Hill f_l and f_v relations for higher and lower initial elevation compared to the periodic orbit starting at $y_0 = 1.042\,\mathrm{m}$: (a) $y_0 = 1.092\,\mathrm{m}$ (b) $y_0 = 1.022\,\mathrm{m}$. Solid black curve is associated with the periodic motion, the dashed orange curves are associated with the perturbed hopping.

Table 3. Optional inputs of the `DynIn` Toolbox.

		Value	
Input parameter	1D	2D	3D
Space boundary	$y \in [l_0, 3\,\mathrm{m}]$	$y \in [0\,\mathrm{m}, 3\,\mathrm{m}]$ $t_a \in [-2.01\,\mathrm{s}, 2.01\,\mathrm{s}]$	$y \in [0\,\mathrm{m}, 3\,\mathrm{m}]$ $t_a \in [-2.01\,\mathrm{s}, 2.01\,\mathrm{s}]$ $\dot{y} \in [-1.1\,\mathrm{m\,s^{-1}}, 1\,\mathrm{m\,s^{-1}}]$
Number of cells	701	701	701
Iteration steps	500	1000	1000

each other, meaning that perturbations considering also the $\dot{y}$ direction do not have greater effect on the dynamical robustness than the perceptional error represented by the disturbance in t_a.

Generally, the limiting factor for the LIM in the 1D case is the distance between the elevation at the flight to stance (D2S) transition and the hopping height of the periodic motion. The exception to this are symmetric systems with constant-linear, Hill-linear and constant-Hill $f_l - f_v$ relations. For these three systems, an unstable periodic orbit exists beside the stable one which limits the value of the LIM. These unstable and stable periodic orbits are represented by fix points in the one-dimensional Poincaré return maps shown in figure 6. For systems not having unstable orbit, greater hopping height means

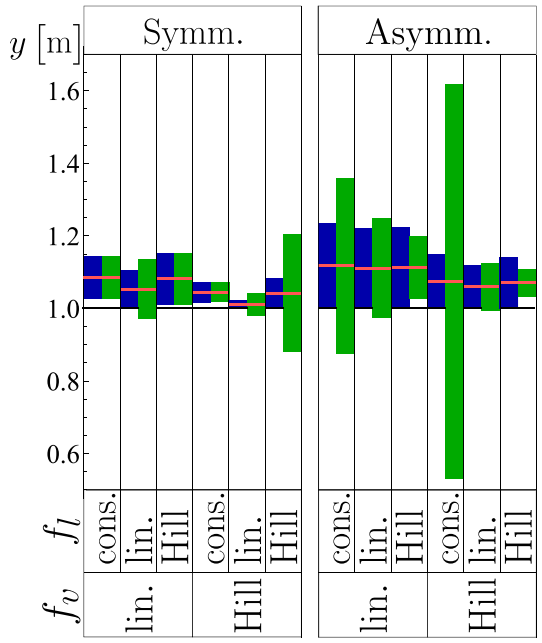

Figure 9. Hyperspheres projected onto the y direction. Red lines denote to the fix point of the periodic motion. Blue bars refer to the LIM_1 values, green bars refer to the LIM_2 values around the fix point. The black horizontal line at $y = 1$ m marks the flight to stance (D2S) transition.

greater LIM_1 value. The value of LIM_1 is also readable from the one-dimensional Poincaré return maps in figure 6.

The hyperspheres of different dimensions are projected onto the y axis for better comparison, as shown in figure 9. The LIM_3 values are not included because they are equal to the LIM_2 values within the error margin of the heuristic approach. As expected, the LIM values generally increase when the ICs are allowed to be chosen from the stance phase as well. However, for asymmetric systems with Hill-linear and Hill-Hill $f_l - f_v$ relations, the LIMs decrease because they are more sensitive to perturbations in the t_a direction (i.e. to perceptual error) than to perturbations in the apex height y_0. For the three systems with an unstable periodic orbit (symmetric systems with constant-linear, Hill-linear and constant-Hill $f_l - f_v$ relations), the LIM values remain unchanged.

In figure 10, simulations are shown for ICs chosen within and outside the two-dimensional hypersphere calculated for the system. Converging and diverging trajectories are illustrated for a symmetric system with linear-Hill $f_l - f_v$ relation in panel (a) and for an asymmetric system with Hill-linear $f_l - f_v$ relation in panel (b). These examples are chosen because their Floquet multipliers μ, and thus their convergence speeds, are similar. However, the diverging trajectories behave differently for the systems. For the symmetric system in panel (a), the diverging trajectory eventually settles into equilibrium. For the asymmetric system in panel (b), the mass collides with the ground because the muscle does not produce enough upward force.

4. Discussion

4.1. The effect of intrinsic muscle properties on hopping heights

All systems were able to produce asymptotically stable hopping motion with approximately 2 Hz frequency. Symmetric systems, which use activation $a_S(t)$, had lower hopping heights compared to asymmetric systems based on [2], which use activation $a_H(t)$. This finding roots in the fact that symmetric systems were not able to produce as great forces as the asymmetric ones due to the characteristics of the f_v functions. The requirement in equation (5) of symmetric behaviour limits the level of muscle activation.

Systems with linear-Hill $f_l - f_v$ relation had the lowest hopping heights compared to any other system with the same activation strategy. Moreover, comparing the group of three systems with different f_l characteristics but same f_v relation and activation strategy, linear f_l yield the lowest while constant f_l results in the highest hopping heights. This is because at zero muscle contraction there is no preload for the linear f_l. Therefore it takes time to build up the force output to match with the forces of systems with constant and Hill f_l characteristics. By examining the muscle characteristics in figure 2 left, the above observation is explained by the fact that linear f_l is the lowest and constant f_l is the highest in the dominant operational range $\Delta l \in [0, 0.1]$ m.

Systems with linear f_v relation were able to hop higher than the systems with Hill f_v relation. As shown in figure 2 right, during the concentric contraction, the values of the linear f_v are higher than the values of the Hill f_v relation. Therefore the system can push the mass upwards with greater force if linear f_v characteristic is used.

4.2. Airborne-ground time

The time period of the hopping is approximately the same for all systems, which implies that the air-ground ratio is less for systems with lower hopping heights, since they spend more time in the stance phase as indicated in figure 5. For running, the efficiency is correlated to the flight time; high-performance runners spend more time in airborne phase at a given speed [43–45]. Therefore systems which are able to produce higher forces thus are able to achieve greater hopping heights are more efficient.

As shown in figure 7, the compression of the muscle of symmetric systems is considerably smaller than that of the asymmetric systems, especially in the case of systems with Hill f_v relation. At the same time, symmetric systems spend more time in the stance phase resulting small acceleration and low muscle forces. This is consistent with the findings in

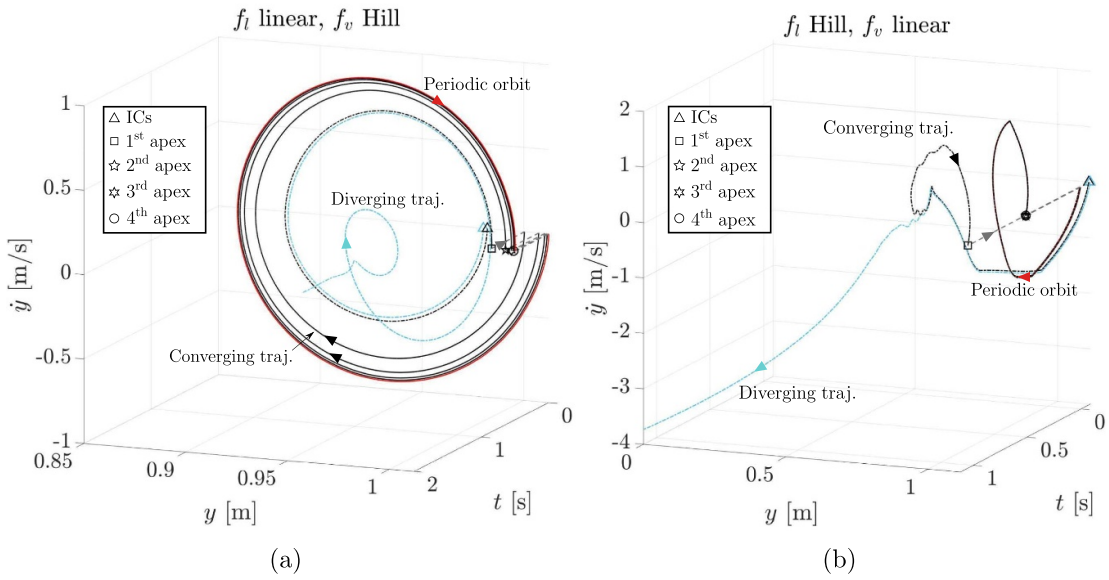

Figure 10. Simulations of converging and diverging trajectories. For all simulations, the initial velocity is $\dot{y}_0 = 0\ [\mathrm{m\,s^{-1}}]$. Panel (a): activation $a_\mathrm{S}(t)$ and initial value $t_{a0} = -0.0017\,[\mathrm{s}]$ are used. The initial positions are $y_{0,\mathrm{c}} = 0.982\,[\mathrm{m}]$ for the converging trajectory and $y_{0,\mathrm{d}} = 0.98\,[\mathrm{m}]$ for the diverging trajectory. Panel (b): activation $a_\mathrm{H}(t)$ and initial value $t_{a0} = -0.0865\,[\mathrm{s}]$ are used. The initial positions are $y_{0,\mathrm{c}} = 1.11\,[\mathrm{m}]$ and $y_{0,\mathrm{d}} = 1.115\,[\mathrm{m}]$ respectively for the converging and diverging trajectories.

[43] related to the gait cycle parameters of slow and fast running.

4.3. Relation of the muscle force and the vertical displacement

The hysteresis seen in figure 7 for asymmetric systems is caused by the f_v characteristic of the muscle. The hysteresis also occurs implicitly in paper [2] in the form of the energy absorbing and generating effect of the muscle. As expected, each symmetric system behaved completely like a spring-mass system while moving on the periodic orbit. This observation is based on that $C_\mathrm{EL} = 1$ for each symmetric system, as shown in table 2. By choosing the activation in a semi-closed form as shown in equation (5), the energy absorbing effect of the f_v relation is eliminated.

According to measurements in [32] hopping with around the preferred 2 Hz or higher frequencies, Farley *et al* found that the body behaves as a simple spring-mass system, based on how the ground reaction force depended on the vertical displacement of the CoM. This behaviour could be modelled by a symmetric system, as the effect of the velocity-force characteristic of the muscles does not appear in the vertical displacement-force relation while moving on the periodic orbit, the system behaves as a simple spring-mass system, as shown in figure 7. As an advantage, the symmetric systems provide asymptotic stability in contrast to a spring-mass system. According to the same measurements in [32], Farley *et al* also stated that in the case of lower hopping frequencies, the vertical displacement of the mass is greater and the body no longer behaves as a spring-mass system. The maximal ground reaction force is measured when the body is moving downwards, and the forces at take-off are higher than at touchdown [32]. These phenomena can also be observed on the asymmetric systems, as shown in figure 7. Therefore on higher frequencies, models with $a_\mathrm{S}(t)$ control approximate more precisely the ground reaction force characteristics, while the force characteristics of asymmetric systems resemble hopping with lower frequencies.

4.4. Energy consumption properties

The mechanical energetic cost of the muscle was calculated for a hopping cycle for each model as table 2 shows. This was used to normalize the potential energy gain as shown in equation (23). Considering systems with constant and Hill f_l characteristics, the values were around 4%–7% greater for asymmetric systems than for the symmetric ones. Symmetric systems had approximately two third as great hopping heights than the asymmetric systems, but they required around two third of muscle work. Thus, the choice between activations $a_\mathrm{S}(t)$ and $a_\mathrm{H}(t)$ did not affect the energy related performance measure P_W. However, significant differences are observed for systems with linear f_l relation. The energy consumption property P_W of the symmetric systems was around 71% and 35% of the asymmetric systems in the case of linear and Hill f_v relations respectively. The energetic cost of the muscle for the symmetric systems was also around two third of the value of the respective asymmetric systems, but the height gain was less than half.

Comparing the systems with the same activation and the same f_l relations, the ones with linear f_v characteristics yielded to higher P_W than systems with Hill f_v relation as table 2 shows. Constant f_l yielded the greatest, linear f_l the lowest energy consumption property P_W for systems with identical control approach and f_v characteristic.

4.5. Dynamical robustness of stable periodic orbits

All asymmetric models have oscillatory convergence and systems with Hill f_v characteristics have faster convergence than the ones with linear f_v relation. Symmetric systems converge the fastest with linear f_l characteristics. The f_v relation has no significant effect on the convergence speed.

The dynamical robustness of the systems were examined through the LIMs around the fix point and was considered in one-, two-, and three-dimensions. Except for three systems, as was mentioned in section 3.3, the limit of the LIM_1 was the flight to stance transition. Therefore the LIM_1 depends on the hopping height; the higher a system is able to hop, the more robust it is. The three symmetric systems with two periodic orbits were exceptions to this. These three systems each had an unstable periodic orbit alongside with the stable one. The unstable periodic orbit had lower hopping heights, which confines the LIM_1 value before the phase transition.

The effect of the perceptional error (i.e. perturbation along the t_a) was taken into account through the two-dimensional LIM. This way, the D2S phase transition no longer restricted the LIM. The LIM_2 value of systems with the unstable periodic orbit was equal to the LIM_1 value, since the limiting factor of the measure was not the eliminated phase transition (see models with red circles in figure 6). Otherwise, the LIM_2 values were greater than the LIM_1 values, except for asymmetric systems with Hill f_l relation. In these two cases, the radius of the hypersphere (LIM_2) along the y direction did not even extend to the phase transition. Therefore, these systems are more sensitive to perceptional errors. Besides, the LIM_2 value has increased greatly for asymmetric systems with constant f_l relation, as well as for the symmetric system with Hill-Hill $f_l - f_v$ characteristics. There were no significant differences between the LIM_2 and LIM_3 values. Thus deviation in the direction of $\dot{y}$ has no greater effect on the robustness than the perceptional error.

The use of the `DynIn` Toolbox has allowed a more complex analysis of the robustness of the systems than the Poincaré return maps. Introducing LIM_2, some models proved to be more robust than in the case when the perturbation is solely considered on the Poincaré section. However, it is important to note that the convergence is not limited to the inside of the hypersphere. The `DynIn` Toolbox offers an upper estimation of a subset of the BoA.

5. Conclusion

Since symmetry is found everywhere in nature, and the elastic muscle model leads to symmetric behaviour, we hypothesised that using a feed-forward control resulting in symmetric motion could offer certain advantages. We investigated the performance of this symmetry inspired controller as a control strategy for hopping robots. Besides, we analysed the resulting system as a feasible model for human hopping motion. To focus on the effect of the feed-forward control, we used a simple one-dimensional hopping model, minimizing the impact of parameter interactions. The intrinsic properties of the Hill muscle model were considered in different complexities, discarding models with constant force-velocity (f_v) relation, since at least linear f_v characteristic is needed for asymptotic stability [2].

The main idea of the study is the proposed closed-form activation function that results in symmetric motion. The compact form of the function makes it easier to find a feed-forward control that yields stable and energy efficient periodic motion, compared to heuristic approaches. Moreover, the effect of the force-velocity relation of the muscle is eliminated while moving on the periodic orbit, allowing the muscle to behave completely elastic, while maintaining asymptotic stability. Systems with the proposed control is compared with systems in [2] through multiple measures, a portion of them are found in [2] and further are introduced in this study. We have concluded that certain measures depend not only on the control strategy, but the intrinsic properties of the muscle model have also great effect. Such hopping characteristic is the hopping height, since the same relation is upheld, regarding the intrinsic properties, among the symmetric and asymmetric systems.

The symmetry requirement limits the force output of the muscle, preventing the symmetric systems from achieving as high hopping height as the asymmetric ones. The behaviour of the symmetric system resembled that of a novice runner comparing its gait cycle parameters to similar parameters describing runners [43]. However, the mechanical energetic cost of the muscle was significantly higher for asymmetric systems. Our investigations found that, considering all the measures analysed, systems with Hill − Hill and constant − linear/Hill $f_l - f_v$ relations were the most advantageous among the symmetric and asymmetric systems, respectively. Since the linear and Hill f_v relations offer different advantages in asymmetric systems, it is not possible to state distinctly which intrinsic characteristic would function superiorly in a robotic controller. The same applies when comparing the symmetric system with the two asymmetric ones. An additional benefit of the closed-form activation is that the numerical cost for optimization is lower than of a heuristic method used in [2].

Humans, considering the ground reaction force-CoM elevation curves, behave like a spring-mass system while hopping at preferred or higher frequencies [32]. The symmetric system could serve as a more sophisticated model for this motion, given its asymptotic stability compared to the marginally stable spring-mass system. On the other hand, the ground reaction force characteristics of lower frequency hopping [32] are well represented by the behaviour of the asymmetric systems.

Data availability statement

All data that support the findings of this study are included within the article (and any supplementary files).

Acknowledgments

The research reported in this paper has been supported by the National Research, Development and Innovation Office (Grant No. NKFI-134496).

Limitations

It is important to note that the muscle model in this study is oversimplified from a physiologically point of view, since the geometry of the leg and the elasticity of the muscle-tendon unit are neglected. Therefore, the mechanical model is not sufficient to study real-life muscle behaviour, or the underlying biomechanics of human hopping. The goal of our study was to examine the effect of different complexities of the CE, while imposing symmetric hopping motion. The findings of this study are useful in the field of robotics, moreover for implementing muscle-like behaviour of robotic actuators.

ORCID iD

Dóra Patkó https://orcid.org/0000-0001-7594-1882

References

[1] Holmes P, Full R J, Koditschek D E and Guckenheimer J 2006 The dynamics of legged locomotion: models, analyses and challenges *SIAM Rev.* **48** 207–304
[2] Häufle D, Grimmer S and Seyfarth A 2010 The role of intrinsic muscle properties for stable hopping-stability is achieved by the force-velocity relation *Bioinspir. Biomim.* **5** 16004
[3] Häufle D, Grimmer S, Kalveram K and Seyfarth A 2012 Integration of intrinsic muscle properties, feed-forward and feedback signals for generating and stabilizing hopping *J. R. Soc. Int. R. Soc.* **9** 1458–69
[4] Hutter M, Remy C D, Hopflinger M A and Siegwart R 2010 Slip running with an articulated robotic leg *The 2010 IEEE/RSJ Int. Conf. on Intelligent Robots and Systems* (*Taipei, Taiwan 18-22 October 2010*) pp 4934–9
[5] Zana R, Bodor B, Bencsik L and Zelei A 2018 A tutorial for the analysis of the piecewise-smooth dynamics of a constrained multibody model of vertical hopping *Math. Comput. Appl.* **23** 74
[6] Zelei A, Krauskopf B, Piiroinen P T and Insperger T 2019 Stable periodic motion of a controlled segmented leg model of pedal locomotion with inelastic ground-foot collision *Nonlinear Dyn.* **97** 1–14
[7] van Soest A J, Bobbert M F and van Ingen Schenau G J 1994 A control strategy for the execution of explosive movements from varying starting positions *J. Neurophys.* **71** 1390–402
[8] Clever D, Hu Y and Mombaur K 2018 Humanoid gait generation in complex environments based on template models and optimality principles learned from human beings *Int. J. Robot. Res.* **37** 1184–204
[9] Navacchia A, Ueno R, Ford K, DiCesare C, Myer G and Hewett T 2019 Emg-informed musculoskeletal modeling to estimate realistic knee anterior shear force during drop vertical jump in female athletes *Ann. Biomed. Eng.* **47** 2416–30
[10] Blickhan R 1989 The spring-mass model for running and hopping *J. Biomech.* **22** 1217–27
[11] Nikooyan N and Zadpoor A 2011 Mass-spring-damper modelling of the human body to study running and hopping - an overview *Proc. Inst. Mech. Eng.* H **225** 1121–35
[12] Oehlke J, Beckerle P, Seyfarth A and Sharbafi M A 2019 Human-like hopping in machines *Biol. Cybern.* **113** 227–38
[13] Zhao G, Mohseni O, Murcia M, Seyfarth A and Ahmad Sharbafi M 2022 Exploring the effects of serial and parallel elasticity on a hopping robot *Front. Neurorobotics* **16** 08
[14] Cavagna G, Heglund N and Taylor C 1977 Mechanical work in terrestrial locomotion: two basic mechanisms for minimizing energy expenditure *Am. J. Physiol.* **233** R243–61
[15] Enoka R 2008 *Neuromechanics of Human Movement* (Human Kinetics)
[16] Hill A V 1938 The heat of shortening and the dynamic constants of muscle *Proc. R. Soc.* B **126** 136–95
[17] van Leeuwen J L 1992 Muscle function in locomotion *Mechanics of animal locomotion* vol 11 pp 191–250
[18] Brown I, Scott S and Loeb G 1995 Preflexes-programmable high-gain zero-delay intrinsic responses of perturbed musculoskeletal systems *Soc. Neurosci. Abstr.* **21** 562.9
[19] Proctor J and Holmes P 2010 Reflexes and preflexes: on the role of sensory feedback on rhythmic patterns in insect locomotion *Biol. Cybern.* **102** 513–31
[20] Geyer H and Seyfarth A 2017 Neuromuscular control models of human locomotion *Humanoid Robotics: A Reference* (Springer) pp 1–30
[21] Brown T G 1914 On the nature of the fundamental activity of the nervous centres; together with an analysis of the conditioning of rhythmic activity in progression and a theory of the evolution of function in the nervous system *J. Physiol.* **48** 18–46
[22] Grillner S 1985 Neurobiological bases of rhythmic motor acts in vertebrates *Science* **228** 143–9
[23] Beer R D 2009 Beyond control: the dynamics of brain-body-environment interaction in motor systems *Adv. Exp. Med. Biol.* **629** 7–24
[24] Orlovsky G, Deliagina T G and Grillner S 1999 *Neuronal Control of Locomotion: from Mollusc to Man* (Oxford University Press) (https://doi.org/10.1093/acprof:oso/9780198524052.001.0001)
[25] Harkema S *et al* 2011 Effect of epidural stimulation of the lumbosacral spinal cord on voluntary movement, standing and assisted stepping after motor complete paraplegia: a case study *Lancet* **377** 1938–47
[26] Dankowicz H and Piiroinen P 2002 Exploiting discontinuities for stabilization of recurrent motions *Dyn. Syst. Int. J.* **17** 317–42
[27] Soliman M S and Thompson J M T 1989 Integrity measures quantifying the erosion of smooth and fractal basins of attraction *J. Sound Vib.* **135** 453–75
[28] Thompson J M T 1989 Chaotic phenomena triggering the escape from a potential well *Proc. R. Soc.* A **421** 195–225

[29] Lenci S and Rega G 2003 Optimal control of homoclinic bifurcation: theoretical treatment and practical reduction of safe basin erosion in the helmholtz oscillator *J. Vib. Control* **9** 281–315
[30] Rega G and Lenci S 2005 Identifying, evaluating and controlling dynamical integrity measures in non-linear mechanical oscillators *Nonlinear Anal. Theory Methods Appl.* **63** 902–14
[31] Habib G 2021 Dynamical integrity assessment of stable equilibria: a new rapid iterative procedure *Nonlinear Dyn.* **106** 1–24
[32] Farley C, Blickhan R, Saito J and Taylor C 1992 Hopping frequency in humans: a test of how springs set stride frequency in bouncing gaits *J. Appl. Physiol.* **71** 2127–32
[33] Alexander R M 2002 Tendon elasticity and muscle function *Comp. Biochem. Physiol.* A **133** 1001–11
[34] Ishikawa M, Komi P V, Grey M J, Lepola V and Bruggemann G-P 2005 Muscle-tendon interaction and elastic energy usage in human walking *J. Appl. Physiol.* **99** 603–8
[35] Wakeling J M, Febrer-Nafría M and De Groote F 2023 A review of the efforts to develop muscle and musculoskeletal models for biomechanics in the last 50 years *J. Biomech.* **155** 111657
[36] Geyer H, Seyfarth A and Blickhan R 2003 Positive force feedback in bouncing gaits? *Proc. Biol. Sci. R. Soc.* **270** 2173–83
[37] Leine R 2000 Bifurcations in discontinuous mechanical systems of the fillippov-type *PhD Thesis 1 (Research TU/e / Graduation TU/e)* Technische Universiteit Eindhoven (https://doi.org/10.6100/IR533239)
[38] Leine R and van Campen D 2002 Discontinuous bifurcations of periodic solutions *Math. Comput. Model.* **36** 259–73
[39] Müller P C 1995 Calculation of lyapunov exponents for dynamic systems with discontinuities *Chaos Solitons Fractals* **5** 1671–81
[40] Lenci S and Rega G 2019 *Global Nonlinear Dynamics for Engineering Design and System Safety* (Springer) (https://doi.org/10.1007/978-3-319-99710-0)
[41] Melvill-Jones G and Watt D 1971 Observations on the control of stepping and hopping movements in man *J. Physiol.* **219** 709–27
[42] Lichtwark G and Wilson A 2005 A modified hill muscle model that predicts muscle power output and efficiency during sinusoidal length changes *J. Exp. Biol.* **208** 2831–43
[43] Novacheck T F 1998 The biomechanics of running *Gait Posture* **7** 77–95
[44] Padulo J, Annino G, Migliaccio G, D'Ottavio S and Tihanyi J 2012 Kinematics of running at different slopes and speeds *J. Strength Cond. Res.* **26** 1331–9
[45] van Oeveren B, de Ruiter C, Beek P and van Dieën J 2021 The biomechanics of running and running styles: a synthesis *Sports Biomech.* **23** 516–54